Sally A. Al-Ani
Mohamed K. Dhahir

Institute of Laser for Postgraduate Studies, University of Baghdad, Al-Jadriya, Baghdad, IRAQ

Effect of Ideal Thickness on Boosting Efficiency of Photoelectrochemical Cell Photoanode via Maximal Absorption

A key role of the thin film is to absorb as much incident light as possible to generate electron-hole pairs for the photoelectrochemical reaction. In this study, we utilize the ability of ideal thickness to optimize the efficiency of PEC cell by designing three photoanodes for an efficient water splitting process. These photoanodes cover the UV, visible, and NIR regions with maximum absorption in a regulated manner. The carefully selected materials that were drop-casted onto the FTO substrate comprised of CeO_2 nanoparticles, copper nanoparticles, and the exclusive material (Epolight™ 1178) as a dye sensitizer. Comprehensive characterization of the photoanode was performed using analytical techniques. Cross-sectional images of the three fabricated photoanodes have been acquired to prove the successful achievement of the ideal thickness requirement which ranged between 8-12 µm. The optical properties were characterized and they prove that for the first photoanode, the maximum absorption peak was at 296 nm, the second absorbs at 294 nm 446, 646, and 709. The third photoanode peaks at 357, 473, 634, and 857 nm covering the three regions. Linear sweep voltammograms were collected in dark and under the illumination of LED source with AM 1.5 G condition at 100 mW/cm^2. The photoanodes exhibited a significant photocurrent response, indicating efficient photoactivity with the current densities of 14.3, 23.0, and 34.2 mA.cm^{-2} at 0.99 V vs. Ag/AgCl for the three photoanodes respectively. A significant enhancement in the efficiency of PEC cell was recorded as it increased from 3.4% to 8.2%.

***Keywords*:** Water-splitting; Photoelectrochemical cell; Linear sweep voltammetry
Received: 12 August 2024; **Revised:** 02 October 2024; **Accepted:** 09 October 2024

1. Introduction

The global energy crisis and environmental concerns have driven the pursuit of sustainable and clean energy sources. Hydrogen (H_2) is considered a promising alternative energy carrier due to its high energy density and its ability to produce water as the only byproduct when used in fuel cells [1,2]. Among various methods of hydrogen production, water splitting using photoelectrochemical (PEC) cells is one of the most attractive, as it directly converts solar energy into hydrogen through the splitting of water molecules. This process offers a renewable and environmentally benign route to generate hydrogen, aligning with global efforts to reduce carbon emissions and dependence on fossil fuels [3,4].

In PEC water splitting, the efficiency of the process hinges on the ability of the photoelectrode materials to absorb sunlight and convert it into charge carriers (electrons and holes) that drive the redox reactions necessary for hydrogen evolution [5-7]. The thickness of the thin film in the photoelectrode plays a critical role in determining light absorption efficiency. Thin films that are too thick can lead to excessive charge carrier recombination, whereas films that are too thin may not absorb enough light to generate a sufficient photocurrent. Hence, optimizing the thin film thickness is crucial to balance light absorption and charge transport, maximizing the overall efficiency of the PEC system [8-10]. For maximal incoming light absorption, a thickness range of 8-12 µm is recommended. Less light is absorbed in a film with a thickness of less than 8 µm due to the material's lower thickness. The films thicker than 12 µm result in increased recombination as the charge carriers must diffuse across the additional layers [11].

In recent years, nanostructured materials have emerged as key players in enhancing PEC cell performance. Among these, cerium dioxide (CeO_2) nanoparticles have garnered attention for their chemical stability, ability to generate oxygen vacancies, and wide bandgap that facilitates the absorption of UV light. However, the limitation of CeO_2 in absorbing only a small portion of the solar spectrum (primarily in the UV range) can hinder its overall efficiency [12,13]. To overcome this, copper (Cu) nanoparticles are often incorporated to enhance light absorption in the visible spectrum through plasmonic effects. The synergistic combination of CeO_2 and Cu nanoparticles can significantly improve the performance of thin films in PEC cells by extending light absorption to a broader wavelength range and enhancing charge separation [14,15]. Incorporating dye materials into this system adds another dimension to enhancing PEC efficiency. The dyes, often used in conjunction with CeO_2 and Cu nanoparticles, help capture visible light, inject excited electrons into the semiconductor, and contribute to improved photocurrent generation. This multilayer approach involving thin films, nanoparticles, and dye sensitization provides a comprehensive strategy to

enhance solar light harvesting and improve hydrogen production [16].

This paper explores the importance of optimizing thin film thickness for maximal light absorption and improved hydrogen production via PEC water splitting. Furthermore, the role of CeO_2 and Cu nanoparticles in enhancing the optical and catalytic properties of thin films are examined, with a focus on their contribution to improving PEC cell efficiency. By understanding the interplay between film thickness and nanomaterial incorporation, we aim to highlight strategies for achieving more efficient hydrogen generation from water splitting.

2. Experimental Part

The main component used to prepare the photoanodes was cerium dioxide nanoparticles (CeO_2 NPs). Cu NPs are involved in both P2 and P3 photoanodes; however, Epolight™ 1178 is a dye material that is only used in P3 production. Deionized (DI) water was used as the solvent for all suspensions. A clean, 1x1 cm^2 piece of glass coated with fluorine tin oxide (FTO) was used as the substrate for each photoanode in order to drop cast the solvents onto the conducting face. A 99.9% pure CeO_2 nanopowder was purchased from Hongwunew Materials. A 0.2g of CeO_2 NPs was dispersed in 25 mL of DI water to form the suspension. The mixture was magnetically stirred for 1 hour at room temperature to ensure proper dispersion of CeO_2 NPs. A micropipette was used to drop-casting 10 drops of the CeO_2 suspension onto the cleaned FTO substrate to form the first layer. Then, the film was allowed to dry on a hot plate. The second layer was created by repeating this method with 10 drops to fabricate the P1 photoanode thin film with two layers of CeO_2 NPs. The P2 photoanode is a two-layer thin film of CeO_2 NPs and Cu NPs, the 99.99% pure Cu nanoparticles were supplied by Nanjing Nano Technology Co. Using the same process in the P1 formation, 10 drops of CeO_2 generate the first layer on an FTO substrate. The second layer was formed by dispersing 0.2 g of Cu NPs in 25 mL of DI water. The suspension was stirred continuously for one hour to achieve a uniform mixture. Following the preparation of the Cu NPs suspension, 10 drops were drop-casted onto the pre-formed CeO_2 layer and dried on a hot plate. P3, the third photoanode is a multi-junction thin film consisted from an FTO substrate, a layer of CeO_2 NPs, a layer of Cu NPs, and a layer of Epolight™ 1178 dye material (CeO_2(NPs)/Cu(NPs)/Epolight™ 1178). The Epolight™ 1178 is a brown dye substance purchased from the Epolin Co. (USA). The method used in the above P2 synthesis was also used to generate the first layer of CeO_2 NPs and the second layer of Cu NPs in this P3 thin film formation, but with 3 and 8 drops of CeO_2 and Cu, respectively. For the final layer, a 0.3g of Epolight™ 1178 dye material was dissolved in 25 mL DI and stirred for 2 hours to form a stable dye solution. Using a micropipette, 5 drops of the dye solution were cast onto the previously deposited CeO_2/Cu bilayer and dried on a hot plate. The formation details are provided in table (1).

The x-ray diffraction (XRD) patterns of CeO_2 NPs and Cu NPs were obtained using Aeris–Malvern Panalytical's X-ray diffractometer. The scanning was over the required range for 2θ values of 15°-75° with ±0.02° peak position accuracy. Peaks of crystalline phases were compared with those of standard compounds of the materials from previous research works.

In order to understand the elemental composition of the Epolight™ 1178 dye material, Axia ChemiSEM was used to perform the energy-dispersive x-ray spectroscopy (EDS). Moreover, top-view SEM and the corresponding EDS mapping images of Epolight™ 1178 were gathered to demonstrate the elemental composition and examine the intense presence of any elemental particles in the material.

The morphological characteristics of the three designed photoanodes P1, P2, and P3 have been detected using FE-SEM InspectTM F50. Cross-sectional FE-SEM images were used to determine the thicknesses of each photoanode.

The optical properties of the three designed photoanodes were investigated using a Shimadzu 1800 UV-VIS-NIR spectrophotometer. This instrument was computerized with a CRT screen and keyboard for operating the input value. The absorption spectra of P1, P2 and P3 were characterized with wavelength range of 190-1100 nm.

The photoelectrochemical (PEC) performances were tested by an electrochemical workstation (ER466, EDAQ potentiostat). Ag/AgCl serves as the reference electrode, Pt serves as the counter electrode, and the three designated photoanodes, P1, P2, and P3, serve as the working electrode in the three-electrode system. Regular testing at room temperature used a 125 mL quartz cell with 2g KOH in DI water with pH of 9, which served as the electrolyte. The linear sweep voltammetry curve was recorded with a scan starting at 0-1 V versus Ag/AgCl. The J-V curves were obtained at a rate of 100 mW/s and at a frequency of 20 kHz at the corresponding program. A light-emitting diode (LED) source (42W, Zethors H7) was used to illuminate the photoanodes under AM 1.5 G condition of 100 mW/cm^2.

3. Results and Discussion

The structural information of CeO_2 NPs and Cu NPs was characterized by powder XRD patterns. Figure (1) displays the pattern of the CeO_2 NPs. It reveals all major peaks of CeO_2 which coincided with lattice planes (111), (200), (220), (311), (222), and (400) and were positioned at 2θ = 28.55°, 33.08°, 47.51°, 56.31°, 59.10° and 69.41°. These findings are identified using the standard JCPDS card no. 34-0394.

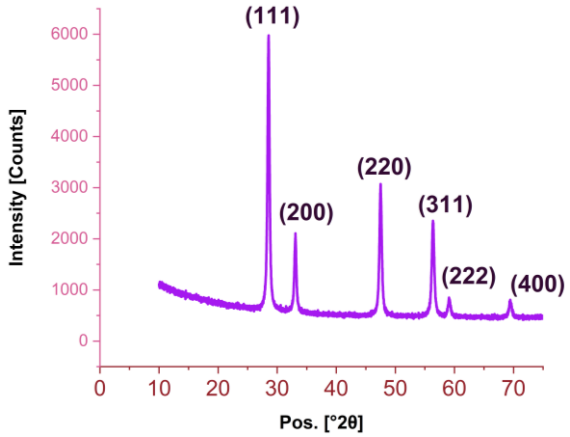

Fig. (1) XRD pattern of CeO_2 NPs

The XRD pattern of Cu NPs is shown in Fig. (2). The typical lines indexed as (111), (200), and (220) that were found at diffraction angles of 43.30°, 50.42° and 74.10°, respectively, correspond to the Cu NPs diffraction peaks which identified using the standard JCPDS card no. 04-0838. A broad diffraction peak of cuprite (111) was observed at a diffraction angle of 36.2°. These diffraction peaks were similar in terms of angular positions to that of FCC pure bulk copper crystalline peaks but were relatively broad, as the mean size of the particles was of the order of nanometers [17].

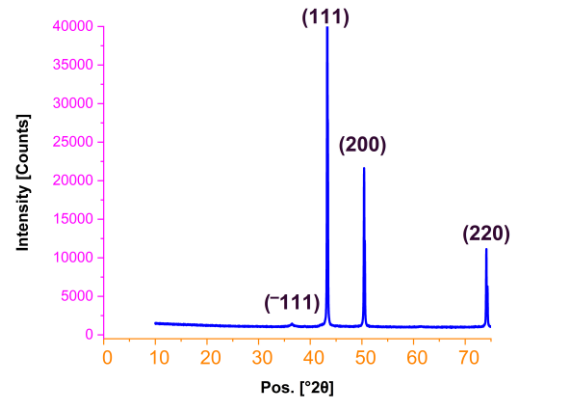

Fig. (2) XRD pattern of Cu NPs

The energy-dispersive x-ray spectroscopy (EDS) analysis is used to characterize the elemental composition of the Epolight™ 1178 dye material and figure (3) shows the EDS elemental analysis data. The results demonstrated that the elements carbon, fluorine, aluminum and antimony were present in high atomic percentages relative to carbon (76.4%). The strong presence of carbon is one of the reasons making Epolight™ 1178 high NIR absorber [18]. Top-view SEM and the corresponding EDS mapping images of Epolight™ 1178 are represented in Fig. (4). From the top-view SEM image, the material size was concluded to be in the micrometer range.

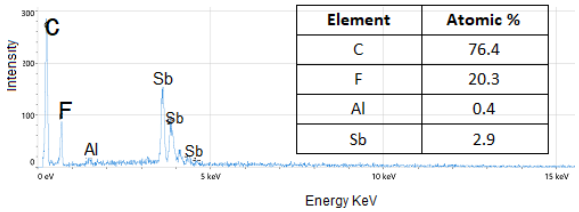

Element	Atomic %
C	76.4
F	20.3
Al	0.4
Sb	2.9

Fig. (3) EDX results of Epolight™ 1178 dye material, indicating that Carbon atoms are distributed in the material with atomic ratios of 76.4%

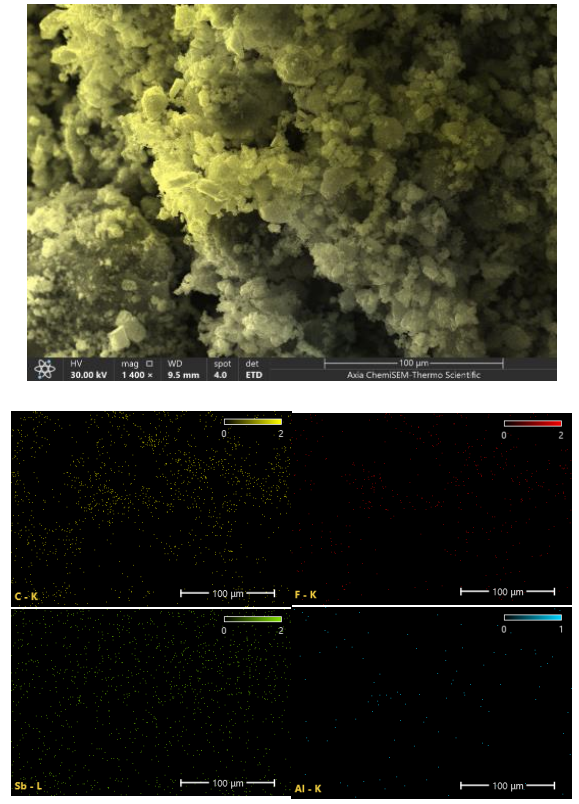

Fig. (4) Top-view SEM and EDS mapping analysis of Epolight™ 1178, the element composition distributions are shown in different colors

Using FE-SEM cross-sectional images of the three fabricated photoanodes have been acquired in order to meet the previously stated required thickness condition for maximal absorption, recommending for a thickness of between 8 and 12 µm for each photoanode. The P1 [FTO/CeO_2(NPs)] photoanode's FE-SEM cross-section image is displayed in Fig. (5a), and it demonstrates that its thickness ranges from roughly 9.3 to 11.6 µm, while the thickness ranged from 9.0 to 12.3 µm for the second photoanode P2 [FTO/CeO_2(NPs)/Cu(NPs)], as can be seen in Fig. (5b). The spherical nature of the copper substance comprising the electrode's second layer can be observed by closely examining the image. Its form differs from that of ceria as well. It should be mentioned that this layer's thickness is roughly equivalent to that of the first layer. The third designed photoanode P3

[FTO/CeO_2(NPs)/Cu(NPs)/Epolight™-1178] had a special situation, since multiple attempts were made to achieve the required thickness. To put it more clearly, when the suspension of EpoliteTM 1178 in DI was drop-casted over the preceding layer of Cu NPs, the so-called coffee ring effect (CRE) was seen. Deegan et al. [19] made notable observations, emphasized, and provided an interpretation of this phenomenon. When the suspended particles form a ring-shaped pattern, the concentrating is near the edges instead of in the center. The CRE is known for its detrimental effects since it tampers with the generally uniform dispersion of particles [20]. The surface tension force of Cu NPs is the primary cause of CRE manifestation in P3.

To address this problem, higher deposits are required, but it's also critical to take the thin film thickness limit into account. Furthermore, the dye material (EpolightTM 1178) is micrometer-sized, therefore, it was required to thin the first layer and create a balance in order to obtain the ideal thickness of the electrode, which is made up of three layers of materials. The P3 photoanode [FTO/CeO_2(NPs)/Cu(NPs)/Epolight^{TM}-1178] cross-sectional image in Fig. (5c) makes this very evident. The thickness of the top layers varied from 9.51 to 11.79 µm, but the initial layer is only 0.457 µm thick, meaning that the overall thickness of the layers is approximately 9.9-12.2 µm.

The results of the thin film thickness for the three fabricated photoanodes P1, P2, and P3 are demonstrated that the thin film's required thickness, which should be between 8 and 12 µm for maximal absorption, was successfully achieved. The photoanodes P1, P2, and P3's absorption spectra were examined in order to assess the absorption enhancement. According to the Fig. (6a) of P1 [FTO/CeO_2(NPs)], there is a strong absorption below 400 nm in the thin film, with a peak at 296 nm. We have related this peak [21] to CeO_2 NPs, which generally exhibit significant absorption peaks in the UV region. The UV-VIS-NIR spectra of the P2 photoanode are shown in Fig. (6b), the bilayer CeO_2(NPs)/Cu(NPs) thin film revealed an optimal light absorption, demonstrated by the three peaks in the visible range (446, 646 and 709 nm) in addition to the peak of 294 nm in the UV region. It is important to mention that, among the above peaks of P2, the 446 nm is the intensive one. It's clearly that the peak at the UV region (294 nm) related to CeO_2 NPs layer, while other peaks are belonging to the Cu NPs, which form the second layer of the P2 photoanode. This may be consistent with studies that have been published regarding Cu NPs absorption peak, which is located at 570 nm [22,23]. Higher efficiency is associated with the appearance of many peaks in the visible region of the absorption spectrum, which are connected to the incorporation of a dielectric semiconductor CeO_2 with a plasmonic Cu nanostructure [24,25]. Because boosting light absorption through metallic enhancement is one method that surface plasmon resonance (SPR) may increase semiconductor photocatalytic activity [25].

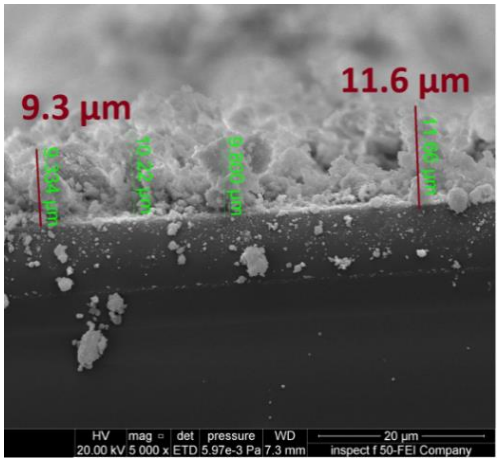

(a)

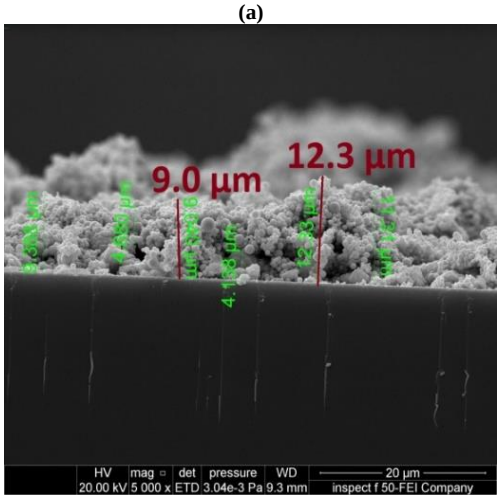

(b)

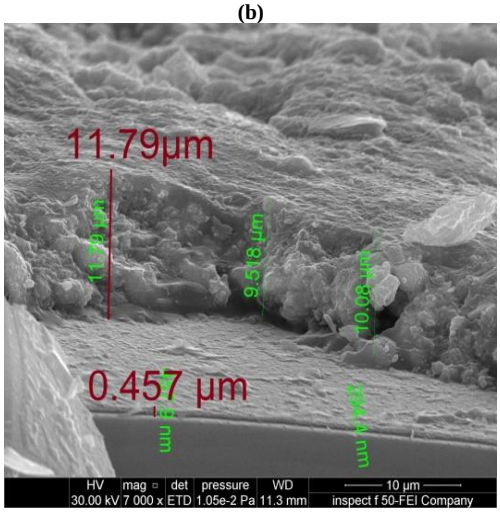

(c)

Fig. (5) Cross-sectional FE-SEM images of (a) P1 [FTO/CeO_2(NPs)] photoanode, (b) P2 [FTO/CeO_2(NPs)/Cu(NPs)] photoanode, (c) P3 [FTO/CeO_2(NPs)/Cu(NPs)/Epolight™-1178] photoanode. The 1st layer thickness is 0.457 µm, the 2nd and 3rd layers thicknesses are ranging from 9.5 to 11.7 µm, and the total thickness of P3 is about 9.9 to 12.2 µm

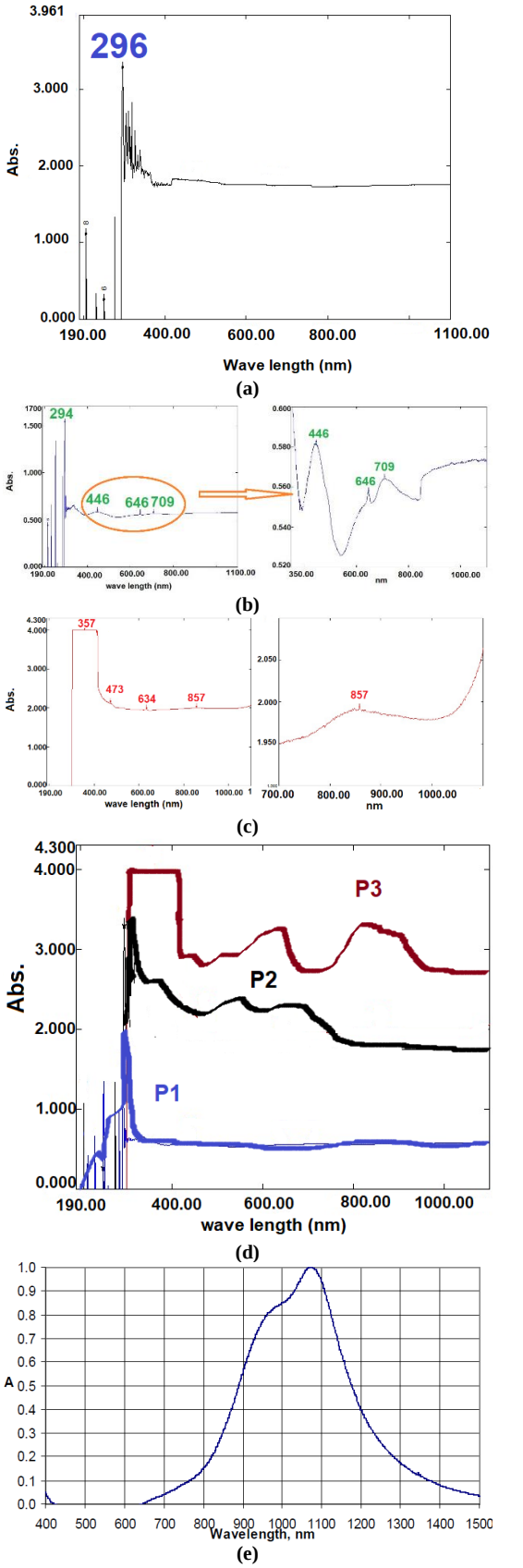

Fig. (6) Absorption spectra of (a) P1, (b) P2 photoanode where the peak at 446nm is the intensive one, (c) P3, and (d) all photoanodes P1, P2, and P3, (e) normalized absorption spectrum of Epolight™ 1178 with λ_{max} at 1073nm

The absorption spectra of the third manufactured photoanode P3, displayed in Fig. (6c), illustrates its significance. Using the unique EpolightTM 1178 dye compound which has a λ_{max} at 1073 nm ensures absorption towards the NIR, which is crucial for creating an effective photoanode. The absorption spectra read a clear absorption peak at 857 nm related to this dye material in addition to the visible and UV peaks, which correspond to CeO_2 NPs and Cu NPs, respectively, at 357 nm, and 473, and 634 nm. Harvesting and using sunlight beyond the UV region is crucial to improve the efficiency of converting light into energy. Further UV-VIS-NIR spectra in Fig. (6d) confirm the existence of longer wavelengths and, consequently, the appearance of spectral redshift. The absorption spectra show excellent absorption enhancement, control over the absorption regions for P1, P2, and P3, and a broad absorption range from the UV to NIR region.

Based on these findings, it can be said that the materials chosen for the three designed photoanodes in addition to their ideal thickness allowed for maximal absorption to be regulated and attained, as shown in table (2). Band alignment and optical properties of photoelectrodes are essential factors for enhancing PEC performance, the band gap energy (E_g) of the thin films was determined from the absorption data using Tauc's equation [26]:

$$\alpha h\nu = A(h\nu - E_{bg})^n \quad (1)$$

where α is the absorption coefficient, h is Planck's constant, ν is the photon frequency, A is the probability parameter for the transition, E_{bg} is the optical bandgap and n related to the transition's type

The optical band gap was obtained from the linear extrapolation of the Tauc's plot for P1 and P3 photoanodes. When $(\alpha h\nu)^2$ is plotted against photon energy ($h\nu$), the intercept of the straight line on the axis matches to the optical band gap (E_g). Plotting this data reveals that P1's E_{bg} is 3.2 eV, as seen in Fig. (7a), related to the CeO_2 material. Reference [27] indicates that the indirect band gap of CeO_2 is 3.2 eV, which is consistent with the previously obtained finding. On the other hand, the energy plotted for P3 is 1.7 eV, as seen in Fig. (7b). As a result, the first and last photoanodes' band gap values reduced from 3.2 to 1.7 eV. The blue shift in energy band gap readings suggests that the Cu NPs and EpolightTM 1178 layers were added, which dramatically reduced the band gap and increased absorption activity, which in turn affected the PEC water splitting efficiency.

As a working electrode, the fabricated photoanodes P1, P2, and P3 were tested with a scan starting at 0-1 V versus Ag/AgCl in the dark. Table (3) illustrates the dark current density of the P1 working electrode increased from $3.2x10^{-3}$ to $5.0x10^{-3}$ mA/cm^2 when the Cu NPs were added as a second layer in P2 thin film fabrication. An increase in conductivity is connected to

this corresponding increase. The dark current is reached to 7.6x10^{-3} mA/cm^2 value for the P3 working electrode.

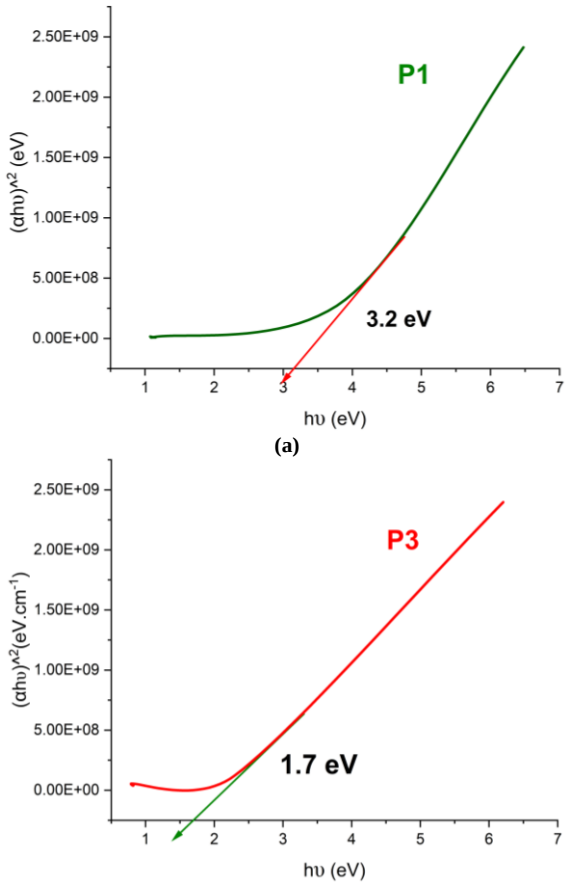

Fig. (7) Determination of optical energy bandgap plotted for (a) P1, and (b) P3 photoanodes

Table (3) Values of the observed dark current of the fabricated photoanodes P1, P2, and P3 at 0.99V vs. Ag/AgCl

Photoanode	Thin film components on a 1x1 cm² FTO substrate	Dark current density at 0.99 V vs. Ag/AgCl (mA/cm²)
P1	CeO_2 NPs	3.2 x10^{-3}
P2	CeO_2(NPs)/Cu(NPs)	5.0 x10^{-3}
P3	CeO_2(NPs)/Cu(NPs)/Epolight™1178	7.6 x10^{-3}

The low current observed in the photoanodes suggests that there aren't numerous defects in the electrode fabrication, which would otherwise cause recombination losses and decreased photoactivity. Due to the differentiation between photocurrent (produced by light-induced processes) and non-photoinduced currents, high dark current may indicate insufficient electrode quality or defective manufacturing, which could have an impact on the PEC cell's overall stability and efficiency.

The study was established by examining the LED illumination influence on P1, P2, and P3 photoanodes, and investigating their behavior. The P1 photoanode [FTO/CeO_2(NPs)] exhibited a current density of 14.3 mA/cm^2 at 0.99 V vs. Ag/AgCl. The positive photogenerated current value indicated that the P1 photoanode was an n-type semiconductor [26,28]. This is consistent with reference [13]. The current density of the second photoanode P2 [FTO/CeO_2(NPs)/Cu(NPs)] is found to be 23.0 mA/cm^2 at 0.99 V vs. Ag/AgCl, while 34.2 mA/cm^2 referred to current density of the third photoanode P3 [FTO/CeO_2(NPs)/Cu(NPs)/Epolight™-1178].

It is noteworthy to emphasis that the LED source was used to simulate the full solar spectrum [29], meaning that the results obtained accurately showed how these photoanodes behaved under solar spectrum characteristics. Additionally, the increase in photocurrent from P1 to P2 to P3 results in a rise in PEC cell efficiency within the solar spectrum (Fig. 8), made this gradual rise in photocurrent density of P1, P2 and P3 under LED illumination very evident. The improvement was made possible by the careful and precise selection of the materials that are utilized in designing these photanodes, as well as their fabrication at the ideal thickness to achieve control of absorption, including highly efficient areas of sunlight and, consequently, a higher current. We notice the increase in photocurrent response was in the form of a bump in peak between 0.55 and 0.75 V of the behavior of the photoanodes. This can be attributed to jumping of the electrons from the valance band to the conduction band till the point of saturation, and then the sharp increase in photocurrent is observed [30].

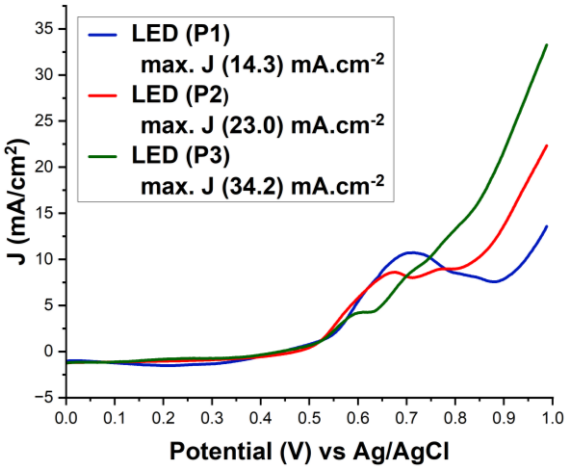

Fig. (8) The I-V curves tested by linear sweep voltammetry under AM 1.5G Illumination of P1, P2 and P3 by LED source

The hydrogen production efficiencies (η) of all the resulted current densities are presented in table (4). In a 3-electrode PEC configuration, when an external bias applying between the working (WE) and the counter electrodes (CE), conversion efficiency is usually evaluated using the equation [31]:

$$\eta = [I\,(1.23 - E_{bias})/\,J_{light}] \times 100\% \qquad (2)$$

where I is photocurrent density at the given potential observed from the experiment (mA/cm^2), E_{bias} is the used potential, 1.23 is the criterion of potential of water splitting, and J_{light} refers the intensity of the irradiating light at 100 mW/cm^2 for AM 1.5 G standard

Table (4) Results of calculated hydrogen production efficiencies for P1, P2 and P3 photoanodes illuminated by different sources

Photoanode	Structure of 1x1 cm² on FTO substrate	Photocurrent density at 0.99 V vs. Ag/AgCl (mA/cm²)	Hydrogen Production Efficiency (η %)
P1	CeO_2 (NPs)	14.3	3.4
P2	CeO_2(NPs)/Cu(NPs)	23.0	5.5
P3	CeO_2(NPs)/Cu(NPs)/ Epolight™-1178	34.2	8.2

Achieving maximum absorption is the main objective for fabricating thin films under the condition of 8-12 µm, further investigation has been established in order to confirm and eliminate doubt with certainty regarding the P1, P2, and P3 thickness. First, the P1 photoanode [FTO/CeO_2(NPs)], which its thickness ranges from 9.3 to 11.6 µm, was selected as the standard sample for this investigation and identified as an S1 sample with a thickness of 11.6 µm. Next, two thin film samples were fabricated to be out of the recommended thickness 8-12 µm, recorded as S2 above the range and S3 below it.

FE-SEM cross sectional images were used to characterize the thickness of S2 and S3 thin films, as illustrated in Fig. (9a and 9b). The S2 thin film had a thickness of 27.57 µm (above the range), while S3 had a thickness of 2.65 µm (below the range).

The absorption measurement conducted on the three models is one of the evaluations that best illustrates the concept of thickness condition. Figure (10) reveals the absorbance of the three samples S1, S2, and S3.

It is evident from the figure that the most intensive sample was S1, which was previously fabricated as P1 with the thickness in the required range as it had an absorbance reach to 3.23. With a thickness over the range, the S2 sample had an absorbance value of 2.35, which was higher than S3's absorbance of 1.48 but lower than S1's. The results displayed in table (5) demonstrated that the thin film which fabricated within the range of 8-12 µm thickness, exhibited the maximal absorbance. This outcome clearly affects the PEC performance of the S1, S2, and S3 samples.

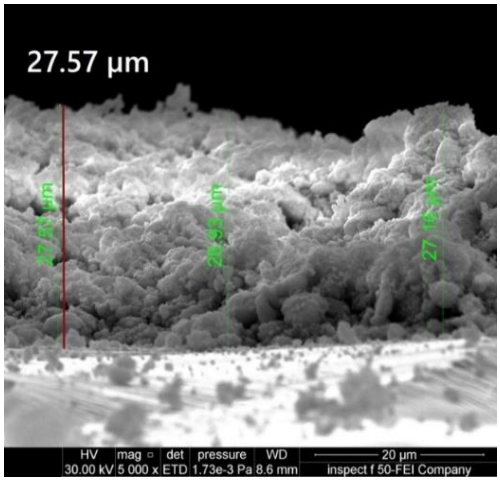

(a)

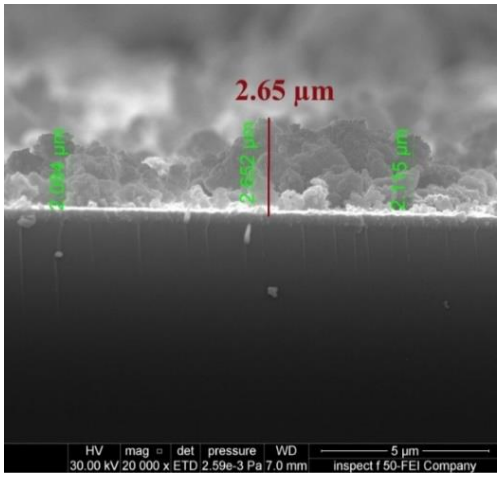

(b)

Fig. (9) Cross-sectional FE-SEM images in comparison to the range 8-12 µm; (a) S2: the thickness is above the range and equal to 27.57 µm, (b) S3: the thickness is below the range and equal to 2.65 µm

Figure (11) shows the I-V characteristic of these samples under LED illumination with AM 1.5 G of 100 mW/cm^2, the current density of S1 (the same of P1) photoanode was previously measured and recorded of 14.3 mA/cm^2 at 0.99 V vs. Ag/AgCl.

The observed current density for S2 and S3 thin films were 7.4 and 4.1 mA/cm^2 at 0.99 V vs. Ag/AgCl, respectively. In practical terms, the results show that for the thin film fabricated within the recommended thickness, the current density recorded the maximum value, and the explanation for this is related to the increasing of the recombination life time with increasing the thin film thickness beyond optimum or recommended thickness [32].

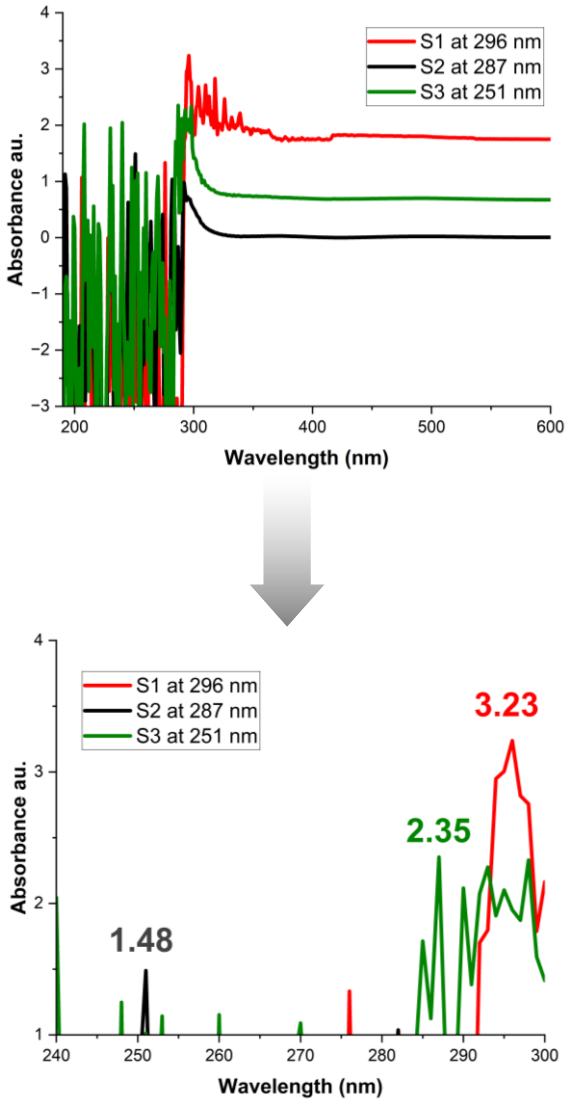

Fig. (10) Absorption spectra of S1, S2, and S3 thin film samples; S1 is the most intensive sample

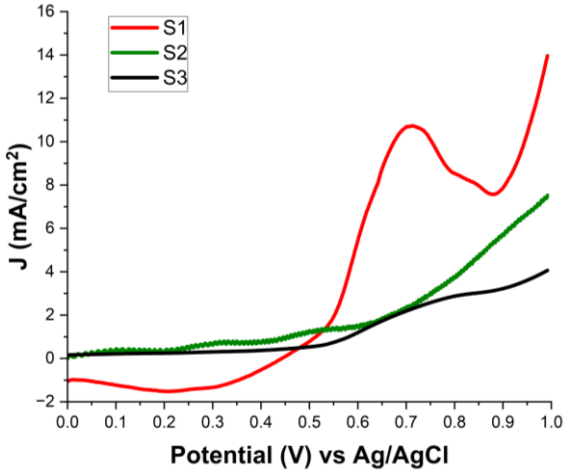

Fig. (11) Comparison of I-V curves tested by linear sweep voltammetry under AM 1.5G Illumination of S1, S2, and S3 thin film samples

4. Conclusions

This research presents the design and fabrication of three optimized and cost effective photoanodes for efficient hydrogen production through PEC water splitting. The study demonstrates that achieving the optimal thickness of photoanode films, which ranged between 8 and 12 µm, is a key factor in enhancing the photocurrent density and overall efficiency of hydrogen production, carefully balancing light absorption to maximize photocurrent density and solar-to-hydrogen (STH) conversion efficiency. Based on the good efficiencies reported of 3.4%, 5.5%, and 8.2% for P1, P2, and P3, respectively, all of the materials used in the three fabricated photoanodes have been found to be appropriate for use as PEC cell photoanodes. It was concluded that for the thin film thickness out of the range, the thin film fabricated above the range has better absorption and performance than the thin film fabricated below the range with the absorbance of 2.35 and 1.48 to the thicknesses 27.57 and 2.65 µm, respectively. The Epolight™ 1178 material is thought to be a great dye sensitizer in the water-splitting PEC field, which significantly affects the third electrode's overall performance, causing a red shift in the absorption range towards the NIR region and producing exceptionally high levels of STH efficiency.

References

[1] A.R. Fareza et al., "Nanoscale metal oxides – 2D materials heterostructures for photoelectrochemical water splitting - a review", *J. Mater. Chem. A*, 10(16) (2022) 8656-8686.

[2] L.H. Razzak, "Current-Voltage Characteristics of Silicon Nitride Nanoparticles Embedded in Porous Silicon Matrix", *Iraqi J. Appl. Phys. Lett.*, 7(3) (2024) 11-14.

[3] F. Mikaeili, T. Gilmore and P. Gouma, "Photochemical Water Splitting via Transition Metal Oxides", *Catalysts*, 12 (2022) 1303.

[4] F.A. Ahmed and A.H. Majeed, "Characteristics of NiO-Doped TeO Thin Films Prepared by Pulsed-Laser Deposition", *Iraqi J. Mater.*, 2(2) (2023) 89-96.

[5] Y. Chiu et al., "Photoelectrochemical cells for solar hydrogen production: Challenges and opportunities", *APL Mater.*, 7 (2019) 080901.

[6] M.B. Costa et al., "Current trending and beyond for solar-driven water splitting reaction on WO_3 photoanodes", *J. Ener. Chem.*, 73 (2022) 88-113.

[7] P. Subramanyam et al., "Emerging materials for plasmon-assisted photoelectrochemical water splitting", *J. Photochem. Photobiol. C: Photochem. Rev.*, 51 (2022) 100472.

[8] M.G. Walter et al., "Solar Water Splitting Cells", *Chem. Rev.*, 110(11) (2010) 6446-6473.

[9] A.Y. Bahlool, "Temperature-Dependent Optoelectronic Characteristics of p-SnO_2/n-Si

Heterojunction Structures", *Iraqi J. Appl. Phys. Lett.*, 7(1) (2024) 23-26.
[10] M.H. Yaseen, R.J. Hameed and A.M. Jasim, "Energy Band Outline of Thin Film CoO:Au/Si Solar Cells", *Iraqi J. Mater.*, 1(2) (2022) 89-94.
[11] W. Jo and R.J. Tayade, "New Generation Energy-Efficient Light Source for Photocatalysis: LEDs for Environmental Applications", *Ind. Eng. Chem. Res*., 53(6) (2014) 2073-2084.
[12] M.S. Anwar et al., "Structural and optical study of samarium doped cerium oxide thin films prepared by electron beam evaporation", *J. Alloys Comp.*, 509 (2011) 4525-4529.
[13] E. Kusmierek, "A CeO_2 Semiconductor as a Photocatalytic and Photoelectrocatalytic Material for the Remediation of Pollutants in Industrial Wastewater: A Review", *Catalysts*, 10 (2020) 1435.
[14] F.G. Hamzah and H.R. Humud, "Signature of Plasmonic Nanostructures Synthesised by Electrical Exploding Wire Technique on Surface-Enhanced Raman Scattering", *Iraqi J. Sci.*, 62 (2021) 167-179.
[15] M.B. Gawande et al., "Cu and Cu-Based Nanoparticles: Synthesis and Applications in Catalysis", *Chem*., 116 (2016) 3722-3811.
[16] K. Hirano, "Sensitization of TiO_2 particles by dyes to achieve H_2 evolution by visible light", *J. Photochem. Photobiol. A: Chem.*, 136(3) (2000) 157-161.
[17] M. Raffi et al., "Investigations into the antibacterial behavior of copper nanoparticles against Escherichia coli", *Ann. Microbiol.*, 60 (2010) 75-80.
[18] D. Han et al., "Thermal properties of carbon black aqueous nanofluids for solar absorption", *Nanoscale Res. Lett.*, 6 (2011) 457.
[19] R.D. Deegan et al., "Capillary flow as the cause of ring stains from dried liquid drops", *Nature*, 592 (2021) 7855.
[20] A.K.S. Kumar et al., "A mini-review: How reliable is the drop casting technique?", *Electrochem. Commun.*, , 121 (2020) 106867.
[21] D. Girija et al., "Cerium oxide nanoparticles – a green, reusable, and highly efficient heterogeneous catalyst for the synthesis of Polyhydroquinolines under solvent-free conditions", *Arch. Appl. Sci. Res.*, 3 (2011) 373-382.
[22] Y. Fan et al., "An overview on water splitting photocatalysts", *Front. Chem. China*, 4 (2009) 4.
[23] M.C. Crisan, M. Teodora and M. Lucian, "Copper Nanoparticles: Synthesis and Characterization, Physiology, Toxicity and Antimicrobial Applications", *Appl. Sci.*, 12 (2022) 141.
[24] J. Li and N. Wu, "Semiconductor-based photocatalysts and photoelectrochemical cells for solar fuel generation: a review", *Catal. Sci. Technol.*, 5 (2014) 3.
[25] S. Cho et al., "Research Update: Strategies for efficient photoelectrochemical water splitting using metal oxide photoanodes", *APL Mater.*, 2 (2014) 010703.
[26] E. D. Palik, **"Handbook of Optical Constants of Solids"**, Academic Press (NY, 1998), 1.
[27] B. Bhushan, **"Springer Handbook of Nanomaterials"**, Springer (Berlin, 2011).
[28] M.L. Gaur et al., "CdSe thin films: morphological, optoelectronic and photoelectrochemical studies", *J. Mater. Sci.: Mater. Electron.*, 25 (2014) 190-195.
[29] W. Jo and R.J. Tayade, "New Generation Energy-Efficient Light Source for Photocatalysis: LEDs for Environmental Applications", *Ind. Eng. Chem. Res*., 53(6) (2014) 2073-2084.
[30] S. Bai et al., "A. An Integrating Photoanode of WO_3/Fe_2O_3 Heterojunction Decorated with NiFe-LDH to Improve PEC Water Splitting Efficiency", *ACS Sustain. Chem. Eng.*, 6 (2018) 12906-12913.
[31] M.A. Green and C.B. Honsberg, **"Handbook of Photovoltaic Science and Engineering"**, John Wiley & Sons (2011).
[32] J.M.K.W. Kumari et al., "The effect of TiO_2 photoanode film thickness on photovoltaic properties of dye-sensitized solar cells", *Ceylon J. Sci.*, 45(1) (2016) 33-41.

Table (1) Materials, concentrations, number of drops that used for the fabricating the three designed photoanodes P1, P2 and P3

Designed photoanode	Layer arrangement	Selected Material	Material Concentration (g)	DI (mL)	No. of Drops
P1	1'st layer	CeO_2(NP)	0.2	25	10
	2'nd layer	CeO_2(NP)			10
P2	1'st layer	CeO_2(NP)	0.2	25	10
	2'nd layer	Cu (NP)	0.2	25	10
P3	1'st layer	CeO_2(NP)	0.2	25	3
	2'nd layer	Cu (NP)	0.2	25	8
	3'rd layer	Epolight™ 1178	0.3	25	5

Table (2) Absorption peaks of the fabricated photoanodes: P1, P2 and P3 with their absorption regions

Photoanode	Thin film components on a (1*1 cm^2) FTO substrate	Thickness achieved in µm	Absorption peaks (nm)
P1	CeO_2(NP)	9.3 – 11.6	296
P2	CeO_2(NP)/Cu(NP)	9.0 – 12.3	294, 446, 646, 709
P3	CeO_2(NP)/Cu(NP)/Epolight™ 1178	9.9 - 12.2	357, 473,634, 857

Table (5) Thin films thicknesses according to the required thickness range 8-12 µm

Thin film Sample	Thin film Component on a 1x1 cm^2 FTO substrate	Resulted thickness in µm	Sample thickness according to the recommended range 8-12µm	Absorbance
S1= P1	CeO_2 (NP)	11.6	Within the range	3.23
S2	CeO_2 (NP)	27.57	Above the range	2.35
S3	CeO_2 (NP)	2.65	Below the range	1.48

